Journal of Applied Mechanics. Received January 26, 2019;
Accepted manuscript posted February 17, 2019. doi:10.1115/1.4042920

A traction-free model for the tensile stiffness and bending stiffness of laminated ribbons of flexible electronics

Shizhen Yin, [a,b] Yewang Su, [a,b,*]

[a] *State Key Laboratory of Nonlinear Mechanics, Institute of Mechanics, Chinese Academy of Sciences, Beijing 100190, China*

[b] *School of Engineering Science, University of Chinese Academy of Sciences, Beijing 100049, China*

[*] To whom all correspondence should be addressed: yewangsu@imech.ac.cn

Journal of Applied Mechanics. Received January 26, 2019;
Accepted manuscript posted February 17, 2019. doi:10.1115/1.4042920

Abstract

Laminated ribbons have been widely adopted for structures of flexible electronics to simultaneously achieve the electronic functions and mechanical performances. Their effective tensile stiffness and bending stiffness, which are extensively used as fundamental parameters in the mechanical analysis, are usually obtained by the plane-strain hypothesis for simplicity. However, it is found that the practical condition is usually closer to the traction free, even for the cases with relatively large width. Here, a traction-free model is proposed to analytically obtain the effective tensile stiffness and bending stiffness of laminated ribbons, which can be used directly in the mechanical analysis of flexible electronics. The prediction of the traction-free model agrees very well with the precise result obtained by 3D FEA for the cases that are in the range of structure designs of flexible electronics. It is found that the tensile/bending stiffness of traction-free model is between the plane-stress model and plane-strain model, but is closer to the plane-stress model. The use of the plane-strain model sometimes may yield considerable error in mechanical analysis of flexible electronics. Parameter study shows that this model is very important for the problems with advanced materials, such as metamaterials with the negative Poisson's ratio. This work provides a theoretical basis for the mechanical analysis of flexible electronics.

Keywords: laminated ribbon, tensile stiffness, bending stiffness, plane-strain, plane-stress, flexible electronics

Journal of Applied Mechanics. Received January 26, 2019;
Accepted manuscript posted February 17, 2019. doi:10.1115/1.4042920

1. Introduction

Flexible electronics have attracted increasing interest in the last decade due to its great potential applications [1, 2]. Examples include electronic eye cameras [3], stretchable electronic skin [4-6], flexible health monitoring system [7-10], stretchable batteries [11], multifunctional integumentary cardiac membranes [12, 13], piezoelectric energy harvesters [14-18], smart gloves for gesture recognition and smart clothing for sitting posture monitoring [19]. More and more studies turn to practical applications [19-21] from ideal concepts of flexible electronics [22-27]. Compared with organic devices, inorganic flexible electronics may achieve practical application earlier, because of their high electronic performance and proven industrial production lines.

Mechanical structural designs, analysis and optimization are critical for the flexibility and stretchability of inorganic electronics [28-30]. The most popular stretchable structure design is the island-bridge mesh structure, as shown in Fig. 1, in which, the functional components reside on the islands and are connected by the stretchable interconnects. The islands do not significantly deform, while the interconnects provide the stretchability for the entire system that is subjected to apparently applied stretch. The geometric design of the interconnects (i.e. bridges) has been developed from straight [31, 32] to curved [33-35] and fractal-inspired [11, 21, 36, 37] layouts; the initial regime of the interconnects has been developed from two dimensional [6] to three dimensional configurations [38]; the deformation mechanism has been developed from buckling [39] to nonbuckling [20]. The stretchability can achieve as large as several hundred percent. For some applications that demand only the bendability rather than stretchability, thin-film-like structures are widely adopted [14, 17]. The thickness of the structure is the key of the design. According to the mechanical analysis, thinner structures usually have better bendability while other parameters are kept.

Laminated ribbons consisting of metals and polymers are widely adopted to simultaneously realize the electronic functions and mechanical bendability and stretchability (Fig. 1) [40-42]. These laminated ribbons usually are subjected to loads of tension and bending. Their effective tensile stiffness and bending stiffness, which are frequently used as fundamental parameters in the mechanical analysis, are usually obtained by the plane-strain hypothesis [14, 15, 17, 40-45]. With this assumption, the strain along the out-of-plane direction (x direction in Fig. 2a) is zero for all layers. The reason of using plane-strain hypothesis is sometimes just for simplicity, or that

Journal of Applied Mechanics. Received January 26, 2019;
Accepted manuscript posted February 17, 2019. doi:10.1115/1.4042920

the width of the ribbon is relatively large. However, the condition of the large width does not ensure the condition of zero strain or zero stress in x direction for all layers. The practical condition in the out-of-plane direction is usually closer to that the apparent traction force and moment (f_x and m_x in Fig. 2a) at the two edges perpendicular to x axis are zero, even for the cases with relatively large width. Therefore, the mechanical condition is neither plane strain nor plane stress, but should be apparent traction free. With the condition of traction free, the interaction between each layer should be quantitatively considered. The detailed analysis will be given in the following section.

In this paper, a traction-free model that is different from both the plane-strain model and the plane-stress model is developed to obtain the effective tensile stiffness and bending stiffness of laminated ribbons, which are frequently used in mechanical analysis of flexible electronic. In section 2, the traction-free model is described and analyzed. Effective tensile stiffness and bending stiffness are obtained analytically. The plane-strain model and the plane-stress model are also analyzed for comparison. In section 3, the traction-free model, the plane-strain model and the plane-stress model are compared systematically with a double-layer example. Finally, concluding remarks are given in Section 4.

2. Analytic models for laminated ribbons

In this section, a traction-free model is proposed to analyze the mechanical behaviors of laminated ribbons. The effective tensile stiffness and bending stiffness are obtained analytically by this model. As illustrated in Fig. 2a, a laminated ribbon of n layers is subjected to the uniformly distributed axial forces f_x and f_z and bending moments m_x and m_z at the boundaries. The relation between the thickness t_i of each layer and the coordinate y_i is $t_i = y_i - y_{i-1}$, as shown in Fig. 2b. With the loads of tension and bending, the principal strains are along the directions of the coordinates. The strains can be obtained by the Kichhoff assumption as

Journal of Applied Mechanics. Received January 26, 2019;
Accepted manuscript posted February 17, 2019. doi:10.1115/1.4042920

$$\begin{cases} \varepsilon_x = \varepsilon_{x0} + \kappa_x \left(y - \frac{1}{2}\sum_{j=1}^{n} t_j \right) \\ \varepsilon_z = \varepsilon_{z0} + \kappa_z \left(y - \frac{1}{2}\sum_{j=1}^{n} t_j \right) \end{cases}, \tag{1}$$

where ε_{x0} and ε_{z0} are the membrane strain at the middle plane ($y = \sum_{j=1}^{n} t_j \big/ 2$) of the laminate ribbon along x and z directions, κ_x and κ_z are the curvatures, respectively. It is worth to notice that the middle plane is not necessary to be the neutral plane for the laminated ribbons with multiple materials, i.e., ε_{x0} and ε_{z0} are not necessary to be zero. The linear elastic constitutive relation gives the normal stresses as

$$\begin{cases} \sigma_x = \frac{E}{1-\nu^2}\left(\varepsilon_x + \nu\varepsilon_z\right) \\ \sigma_z = \frac{E}{1-\nu^2}\left(\varepsilon_z + \nu\varepsilon_x\right) \end{cases}. \tag{2}$$

Here, E is Young's modulus and ν is Poisson's ratio. Therefore, the axial forces and bending moments per unit length can be obtained by the integration over the entire thickness of the laminated ribbons,

$$\begin{aligned} f_x &= \int_{y_0}^{y_n} \sigma_x dy \\ f_z &= \int_{y_0}^{y_n} \sigma_z dy \\ m_x &= \int_{y_0}^{y_n} \sigma_x \left(y - \frac{1}{2}\sum_{j=1}^{n} t_j \right) dy \\ m_z &= \int_{y_0}^{y_n} \sigma_z \left(y - \frac{1}{2}\sum_{j=1}^{n} t_j \right) dy \end{aligned}. \tag{3}$$

Substitution of Eqs. (1) and (2) into Eq. (3) gives the relation between the axial forces/bending moments and the membrane strains/curvatures as

$$\begin{bmatrix} f_x \\ f_z \\ m_x \\ m_z \end{bmatrix} = \begin{bmatrix} \alpha_1 & \alpha_2 & \alpha_3 & \alpha_4 \\ \alpha_2 & \alpha_1 & \alpha_4 & \alpha_3 \\ \alpha_3 & \alpha_4 & \alpha_5 & \alpha_6 \\ \alpha_4 & \alpha_3 & \alpha_6 & \alpha_5 \end{bmatrix} \begin{bmatrix} \varepsilon_{x0} \\ \varepsilon_{z0} \\ \kappa_x \\ \kappa_z \end{bmatrix}, \tag{4}$$

Journal of Applied Mechanics. Received January 26, 2019;
Accepted manuscript posted February 17, 2019. doi:10.1115/1.4042920

where

$$
\begin{aligned}
&\alpha_1=\sum_{i=1}^{n}\frac{E_i t_i}{1-\nu_i^2}\\
&\alpha_2=\sum_{i=1}^{n}\frac{\nu_i E_i t_i}{1-\nu_i^2}\\
&\alpha_3=\sum_{i=1}^{n}\frac{E_i t_i}{2\left(1-\nu_i^2\right)}\left(\sum_{j=1}^{i-1}t_j+\sum_{j=1}^{i}t_j-\sum_{j=1}^{n}t_j\right)\\
&\alpha_4=\sum_{i=1}^{n}\frac{\nu_i E_i t_i}{2\left(1-\nu_i^2\right)}\left(\sum_{j=1}^{i-1}t_j+\sum_{j=1}^{i}t_j-\sum_{j=1}^{n}t_j\right)\\
&\alpha_5=\sum_{i=1}^{n}\frac{E_i}{3\left(1-\nu_i^2\right)}\left\{\left[\left(\sum_{j=1}^{i}t_j-\frac{1}{2}\sum_{j=1}^{n}t_j\right)^3-\left(\sum_{j=1}^{i-1}t_j-\frac{1}{2}\sum_{j=1}^{n}t_j\right)^3\right]\right\}\\
&\alpha_6=\sum_{i=1}^{n}\frac{\nu_i E_i}{3\left(1-\nu_i^2\right)}\left\{\left[\left(\sum_{j=1}^{i}t_j-\frac{1}{2}\sum_{j=1}^{n}t_j\right)^3-\left(\sum_{j=1}^{i-1}t_j-\frac{1}{2}\sum_{j=1}^{n}t_j\right)^3\right]\right\}
\end{aligned}
\quad . \tag{5}
$$

Here, E_i, ν_i and t_i are Young's modulus, Poisson's ratio and thickness of the ith layer in the laminated structure, respectively. With the traction-free condition at the boundaries that are perpendicular to x axis

$$f_x=m_x=0 \tag{6}$$

and zero bending moment condition

$$m_z=0\,, \tag{7}$$

the tensile stiffness is obtained as

$$\overline{EA}_{z,traction-free}=\frac{f_z}{\varepsilon_{z0}}=\frac{\left(\alpha_1\alpha_5+\alpha_2\alpha_6-\alpha_3^2-\alpha_4^2\right)^2-\left(\alpha_1\alpha_6+\alpha_2\alpha_5-2\alpha_3\alpha_4\right)^2}{\alpha_1\left(\alpha_5^2-\alpha_6^2\right)-\alpha_5\left(\alpha_3^2+\alpha_4^2\right)+2\alpha_3\alpha_4\alpha_6}. \tag{8}$$

With the traction-free conditions (6) and zero force condition

$$f_z=0\,, \tag{9}$$

the bending stiffness is obtained as

$$\overline{EI}_{z,traction-free}=\frac{m_z}{\kappa_z}=\frac{\left(\alpha_1\alpha_5+\alpha_2\alpha_6-\alpha_3^2-\alpha_4^2\right)^2-\left(\alpha_1\alpha_6+\alpha_2\alpha_5-2\alpha_3\alpha_4\right)^2}{\alpha_5\left(\alpha_1^2-\alpha_2^2\right)-\alpha_1\left(\alpha_3^2+\alpha_4^2\right)+2\alpha_2\alpha_3\alpha_4}. \tag{10}$$

In the plane-strain model, $\varepsilon_x=\varepsilon_{x0}+\kappa_x\left(y-\sum_{j=1}^{n}t_j\Big/2\right)=0$ is required. The traction-free model can be degenerated to plane-strain model by applying the condition

Journal of Applied Mechanics. Received January 26, 2019;
Accepted manuscript posted February 17, 2019. doi:10.1115/1.4042920

$$\varepsilon_{x0} = \kappa_x = 0 \tag{11}$$

to the above derivations. In conventional derivation of plane-strain tensile stiffness, the effect of bending is not considered. By applying the additional condition $\kappa_z = 0$, the tensile stiffness of plane-strain model can be obtained as

$$\overline{EA}_{z,plane-strain} = \alpha_1 = \sum_{i=1}^{n} \frac{E_i t_i}{1-\nu_i^2} . \tag{12}$$

With the traction-free condition (11), the bending stiffness then degenerates to

$$\overline{EI}_{z,plane-strain} = \alpha_5 - \frac{\alpha_3^2}{\alpha_1} . \tag{13}$$

Replacing $E_i \big/ \left(1-\nu_i^2\right)$ by E_i, in Eqs. (5), (12) and (13), the tensile stiffness and bending stiffness for the plane-stress model are obtained as

$$\overline{EA}_{z,plane-stress} = \alpha_1' = \sum_{i=1}^{n} E_i t_i \tag{14}$$

and

$$\overline{EI}_{z,plane-strain} = \alpha_5' - \frac{\left(\alpha_3'\right)^2}{\alpha_1'} \tag{15}$$

where

$$\begin{aligned} \alpha_1' &= \sum_{i=1}^{n} E_i t_i \\ \alpha_3' &= \sum_{i=1}^{n} \frac{E_i t_i}{2} \left(\sum_{j=1}^{i-1} t_j + \sum_{j=1}^{i} t_j - \sum_{j=1}^{n} t_j \right) \\ \alpha_5' &= \sum_{i=1}^{n} \frac{E_i}{3} \left\{ \left[\left(\sum_{j=1}^{i} t_j - \frac{1}{2} \sum_{j=1}^{n} t_j \right)^3 - \left(\sum_{j=1}^{i-1} t_j - \frac{1}{2} \sum_{j=1}^{n} t_j \right)^3 \right] \right\} \end{aligned} . \tag{16}$$

There are two special cases that should be discussed here:

1) For $\nu_i = \nu$, i.e., the Poisson's ratio of each layer is the same. The coefficient α_i in Eq. (5) degenerates to

$$\alpha_1 = \frac{1}{1-\nu^2}\alpha_1',\ \alpha_2 = \frac{\nu}{1-\nu^2}\alpha_1',\ \alpha_3 = \frac{1}{1-\nu^2}\alpha_3',\ \alpha_4 = \frac{\nu}{1-\nu^2}\alpha_3',\ \alpha_5 = \frac{1}{1-\nu^2}\alpha_5',\ \alpha_6 = \frac{\nu}{1-\nu^2}\alpha_5' . \tag{17}$$

The bending stiffness of traction-free model given in Eq. (10) degenerates to Eq. (15) that is for the plane-stress model. Similar to the derivation of Eq. (8), the tensile stiffness of traction–free

Journal of Applied Mechanics. Received January 26, 2019;
Accepted manuscript posted February 17, 2019. doi:10.1115/1.4042920

model degenerates to Eq. (14) that is for the plane-stress model, by application of the additional condition $\kappa_z = 0$.

2) For $\nu_i = 0$, i.e., the Poisson's ratio of each layer is zero. The coefficient α_i in Eq. (5) degenerates to

$$\alpha_1 = \frac{1}{1-\nu^2}\alpha_1',\ \alpha_2 = 0,\ \alpha_3 = \frac{1}{1-\nu^2}\alpha_3',\ \alpha_4 = 0,\ \alpha_5 = \frac{1}{1-\nu^2}\alpha_5',\ \alpha_6 = 0. \quad (18)$$

The bending stiffness of the three models becomes completely the same. With the application of the additional condition $\kappa_z = 0$ to the traction-free model, the tensile stiffness of the three models also agree with each other.

3. Results and discussions

In this section, the traction-free model, the plane-strain model and the plane-stress model are compared systematically with an example of a double-layer ribbon. The underlying mechanism that yields the difference among the models is investigated. Effects of the parameters, such as the width of the ribbon, the Young's modulus and the Poisson's ratio on the tensile stiffness and the bending stiffness are studied comprehensively. Finite element analysis (FEA) with three-dimensional (3D) practical conditions is conducted to verify the results.

The cross section of the double-layer ribbon with width w, thickness t_i, Young's modulus E_i and Poisson's ratio ν_i for the *i*th layer, is shown in Fig. 3a. To study the tensile stiffness, a uniformly distributed tensile force f_z is applied to the two ends of the ribbon while other forces and moments are zero (Fig. 2a). For the bending stiffness, a uniformly distributed bending moment m_z is applied to the two ends of the ribbon while other forces and moments are zero (Fig. 2a). With the thicknesses $t_1 = t_2 = 1\ \mu\text{m}$, the Young's moduli $E_1 = E_2 = 1\ \text{GPa}$ and the Poisson's ratios $\nu_1 = 0, \nu_2 = 0.49$, the comparison of tensile/bending stiffness of the three models and the effects of the width w are depicted in Figs. 3b1/3b2, respectively. For all the range of the width w, the tensile/bending stiffness per width of the traction-free model is between that of the plane-stress model and the plane-strain model. The precise result predicted by FEA (see the next paragraph for detail) verified the traction-free model. For $w > 10\ \mu\text{m}$ that is in the range

Journal of Applied Mechanics. Received January 26, 2019;
Accepted manuscript posted February 17, 2019. doi:10.1115/1.4042920

of structure designs of flexible electronics, the tensile/bending stiffness resulted from the traction-free model agrees very well with the FEA prediction, while the precise result approaches the plane-stress model for narrower width w. For a small width w, the deformation mode of most region does not keep the Kichhhoff assumption, and the result of 3D FEA for practical conditions deviates from the traction-free model and approaches that of the plane-stress model. Moreover, the result of the traction-free model is closer to that of the plane-stress model, instead of the plane-strain model that has been usually adopted in the past mechanical analysis for simplicity [14, 15]. With the development of the material science, metamaterials with extreme mechanical properties are widely utilized in advanced structures and devices. In this context, the case with $\nu_1 = -0.9$ and $\nu_2 = 0.49$ is studied in Fig. 3c1/3c2. The tensile/bending stiffness of the plane-strain model is more than three/two times as large as that of the plane-stress model, while the traction-free model is closer to the plane-stress model.

In the model of FEA, 3D solid element with real dimensions and material parameters is used to simulate the practical conditions. The stress-free condition is applied at the two edges perpendicular to x axis (Fig. 2a), as well as the bottom and top surface. Because the tensile/bending stiffness should be independent of the length of the model, the hypothesis of the plane section is kept at the two edges perpendicular to z axis (Fig. 2a), by using of the 'reference point', the 'rigid plane' and the 'non-friction contact' in the commercial software ABAQUS [46]. With these conditions, the hypothesis of plane section (x-y plane) is kept everywhere along z axis, while the interaction between adjacent layers appears along x axis.

To understand the underlying mechanism that yields the difference among the three models, the distribution of the shear stress τ_{xy} at the interface between the two layers is studied with the example of the tension of the double-layer ribbon. For the plane-strain model, there is no shear stress τ_{xy} at the interface between adjacent layers, which is ensured by the condition of zero strain ε_{xx} for each layer. The 'constraint' along x direction is very 'strong'. In the plane-stress model, the condition of zero stress σ_{xx} is confirmed, and the deformation in x direction is free and independent for each layer. Shear stress τ_{xy} is also zero or not considered in fact. The 'constraint' along x direction is 'zero'. In the traction-free model, the condition of

Journal of Applied Mechanics. Received January 26, 2019;
Accepted manuscript posted February 17, 2019. doi:10.1115/1.4042920

zero traction force and moment is ensured anywhere along x axis, while shear stress between the adjacent layers locates near the two boundaries, as shown in Fig. 4. The 'constraint' of along x direction is very 'weak'. The order of the 'constraint' of the three models corresponds to the order of the amplitude of the tensile stiffness, as shown in Figs. 3b1, 3b2, 3c1&3c2. Figure 4a shows the distribution of the shear stress τ_{xy} normalized by the applied stress σ_{zz} obtained by the 3D FEA with practical conditions. For small width ($w <\sim 3\ \mu\text{m}$), the shear stress distributes in the entire width and the peak is relatively small. The traction-free model approaches the plane-stress model, which is confirmed by the 3D FEA (Fig. 3). For larger width ($w >\sim 3\ \mu\text{m}$), the nonzero shear stress distributes mainly at the area near the two boundaries. This point can be further shown in Fig. 4b. The shear stress τ_{xy} transfers and balances the normal stress σ_{xx} of the two layers in a transferring region with the size of $r_{transfer}$. When the width w reaches a certain large value, the peak of shear stress becomes a constant $\tau_{\max}$, which is independent of the width w. The transferring region $r_{transfer}$ can be defined as the size of the region where $\tau_{xy}/\tau_{\max} \geq 1\%$. As shown in Fig. 4b, $r_{transfer}$ increases with the increase of the width w at the beginning and becomes constant when w is large. For the extreme case with $\nu_1 = -0.9$ and $\nu_2 = 0.49$, the peaks of the shear stress becomes much larger as depicted in Fig. 4c, because the deformation of the two layers becomes more uncoordinated.

Furthermore, the effects of mechanical property and geometry on the tensile/bending stiffness are also discussed for the three analytical models. Firstly, the effect of Poisson's ratio is studied as shown in Fig. 5. For the given Poisson's ratio $\nu_1 = -0.9,\ 0$ and 0.5, respectively, the tensile/bending stiffness as a function of ν_2 is compared for the three models. The result of the plane-stress model is independent of the Poisson's ratio ν_1 and ν_2. For $\nu_1 = -0.9$, the tensile/bending stiffness of the plane-strain model is much larger than that of the traction-free model and the plane-stress model (Fig. 5a1/5a2). The result of the traction-free model approaches that of plane-stress model for $\nu_1 = \nu_2 = -0.9$ (Figs. 5a1/5a2) and $\nu_1 = \nu_2 = 0.5$ (Fig.

Journal of Applied Mechanics. Received January 26, 2019;
Accepted manuscript posted February 17, 2019. doi:10.1115/1.4042920

5c1/5c2), respectively. For $\nu_1 = 0$ as shown in Fig. 5b1/5b2, the results of the three models approach to each other for $\nu_2 = 0$. The effects of Young's modulus E_2 and thickness t_2 are also studied in Fig. 6. The tensile/bending stiffness here is normalized by that of the plane-stress model. The results confirmed that the traction-free model can give the accurate prediction of the tensile/bending stiffness for laminated ribbons of flexible electronics, while those from the plane-strain model and the plane-stress model are not good enough.

4. Concluding remarks

1) The effective tensile/bending stiffness of laminated ribbons, which is frequently used as the fundamental parameter in the mechanical analysis of flexible electronics, is usually obtained by the plane-strain hypothesis for simplicity. It is found that the practical condition is usually closer to the traction free instead of the plane strain, even for the cases with relatively large width.
2) A traction-free model is proposed to study the effective tensile/bending stiffness of the laminated ribbon. Analytic expressions for the effective tensile/bending stiffness are obtained, which can be used directly in the mechanical analysis of flexible electronics.
3) The prediction of the traction-free model agrees very well with the precise result, which is obtained by 3D FEA for the cases in the range of structure designs of flexible electronics. It shows the validation of the application of the traction-free model to flexible electronics.
4) For all the cases we have studied, the result of the traction-free model is between the plane-stress model and the plane-strain model, but is closer to the plane-stress model. The use of the plane-strain model sometimes may yield considerable error in mechanical analysis of flexible electronics.
5) Effects of the Poisson's ratio, Young's modulus and the ribbon thickness are studied systematically. It shows that this work is very important for the problems with advanced materials, such as metamaterials with the negative Poisson's ratio.

Acknowledgements

The authors gratefully acknowledge the support from the National Natural Science Foundation of China (grants 11772331 and 11572323), Chinese Academy of Sciences via the "Hundred Talent

Journal of Applied Mechanics. Received January 26, 2019;
Accepted manuscript posted February 17, 2019. doi:10.1115/1.4042920

Program", Strategic Priority Research Program of the Chinese Academy of Sciences (No. XDB22040501).

Journal of Applied Mechanics. Received January 26, 2019;
Accepted manuscript posted February 17, 2019. doi:10.1115/1.4042920

Reference

[1] Rogers, J. A., Someya, T., and Huang, Y., 2010, "Materials and Mechanics for Stretchable Electronics," Science, 327(5973), pp. 1603-1607.

[2] Hu, J., Li, R., Liu, Y., and Su, Y., 2018, "An overview of healthcare monitoring by flexible electronics," Science China-Physics Mechanics & Astronomy, 61(9).

[3] Ko, H. C., Stoykovich, M. P., Song, J., Malyarchuk, V., Choi, W. M., Yu, C.-J., Geddes, J. B., III, Xiao, J., Wang, S., Huang, Y., and Rogers, J. A., 2008, "A hemispherical electronic eye camera based on compressible silicon optoelectronics," Nature, 454(7205), pp. 748-753.

[4] Wagner, S., Lacour, S. P., Jones, J., Hsu, P.-h. I., Sturm, J. C., Li, T., and Suo, Z., 2004, "Electronic skin: architecture and components," Physica E: Low-dimensional Systems and Nanostructures, 25(2-3), pp. 326-334.

[5] Hammock, M. L., Chortos, A., Tee, B. C., Tok, J. B., and Bao, Z., 2013, "25th anniversary article: The evolution of electronic skin (e-skin): a brief history, design considerations, and recent progress," Advanced materials, 25(42), pp. 5997-6038.

[6] Kim, D. H., Lu, N. S., Ma, R., Kim, Y. S., Kim, R. H., Wang, S. D., Wu, J., Won, S. M., Tao, H., Islam, A., Yu, K. J., Kim, T. I., Chowdhury, R., Ying, M., Xu, L. Z., Li, M., Chung, H. J., Keum, H., McCormick, M., Liu, P., Zhang, Y. W., Omenetto, F. G., Huang, Y. G., Coleman, T., and Rogers, J. A., 2011, "Epidermal Electronics," Science, 333(6044), pp. 838-843.

[7] Jang, K.-I., Li, K., Chung, H. U., Xu, S., Jung, H. N., Yang, Y., Kwak, J. W., Jung, H. H., Song, J., Yang, C., Wang, A., Liu, Z., Lee, J. Y., Kim, B. H., Kim, J.-H., Lee, J., Yu, Y., Kim, B. J., Jang, H., Yu, K. J., Kim, J., Lee, J. W., Jeong, J.-W., Song, Y. M., Huang, Y., Zhang, Y., and Rogers, J. A., 2017, "Self-assembled three dimensional network designs for soft electronics," Nature Communications, 8.

[8] Kim, D. H., Wang, S., Keum, H., Ghaffari, R., Kim, Y. S., Tao, H., Panilaitis, B., Li, M., Kang, Z., Omenetto, F., Huang, Y., and Rogers, J. A., 2012, "Thin, flexible sensors and actuators as 'instrumented' surgical sutures for targeted wound monitoring and therapy," Small, 8(21), pp. 3263-3268.

[9] Dagdeviren, C., Su, Y. W., Joe, P., Yona, R., Liu, Y. H., Kim, Y. S., Huang, Y. A., Damadoran, A. R., Xia, J., Martin, L. W., Huang, Y. G., and Rogers, J. A., 2014, "Conformable amplified lead zirconate titanate sensors with enhanced piezoelectric response for cutaneous pressure

Journal of Applied Mechanics. Received January 26, 2019;
Accepted manuscript posted February 17, 2019. doi:10.1115/1.4042920

monitoring," Nature Communications, 5.

[10] Fan, J. A., Yeo, W.-H., Su, Y., Hattori, Y., Lee, W., Jung, S.-Y., Zhang, Y., Liu, Z., Cheng, H., Falgout, L., Bajema, M., Coleman, T., Gregoire, D., Larsen, R. J., Huang, Y., and Rogers, J. A., 2014, "Fractal design concepts for stretchable electronics," Nature Communications, 5.

[11] Xu, S., Zhang, Y., Cho, J., Lee, J., Huang, X., Jia, L., Fan, J. A., Su, Y., Su, J., Zhang, H., Cheng, H., Lu, B., Yu, C., Chuang, C., Kim, T.-i., Song, T., Shigeta, K., Kang, S., Dagdeviren, C., Petrov, I., Braun, P. V., Huang, Y., Paik, U., and Rogers, J. A., 2013, "Stretchable batteries with self-similar serpentine interconnects and integrated wireless recharging systems," Nature Communications, 4.

[12] Su, Y., Liu, Z., and Xu, L., 2016, "An Universal and Easy-to-Use Model for the Pressure of Arbitrary-Shape 3D Multifunctional Integumentary Cardiac Membranes," Advanced Healthcare Materials, 5(8), pp. 889-892.

[13] Xu, L., Gutbrod, S. R., Bonifas, A. P., Su, Y., Sulkin, M. S., Lu, N., Chung, H.-J., Jang, K.-I., Liu, Z., Ying, M., Lu, C., Webb, R. C., Kim, J.-S., Laughner, J. I., Cheng, H., Liu, Y., Ameen, A., Jeong, J.-W., Kim, G.-T., Huang, Y., Efimov, I. R., and Rogers, J. A., 2014, "3D multifunctional integumentary membranes for spatiotemporal cardiac measurements and stimulation across the entire epicardium," Nature Communications, 5.

[14] Dagdeviren, C., Yang, B. D., Su, Y. W., Tran, P. L., Joe, P., Anderson, E., Xia, J., Doraiswamy, V., Dehdashti, B., Feng, X., Lu, B. W., Poston, R., Khalpey, Z., Ghaffari, R., Huang, Y. G., Slepian, M. J., and Rogers, J. A., 2014, "Conformal piezoelectric energy harvesting and storage from motions of the heart, lung, and diaphragm," Proceedings of the National Academy of Sciences of the United States of America, 111(5), pp. 1927-1932.

[15] Su, Y. W., Dagdeviren, C., and Li, R., 2015, "Measured Output Voltages of Piezoelectric Devices Depend on the Resistance of Voltmeter," Advanced Functional Materials, 25(33), pp. 5320-5325.

[16] Su, Y. W., Li, S. A., Li, R., and Dagdeviren, C., 2015, "Splitting of neutral mechanical plane of conformal, multilayer piezoelectric mechanical energy harvester," Applied Physics Letters, 107(4).

[17] Dagdeviren, C., Hwang, S.-W., Su, Y., Kim, S., Cheng, H., Gur, O., Haney, R., Omenetto, F. G., Huang, Y., and Rogers, J. A., 2013, "Transient, Biocompatible Electronics and Energy

Journal of Applied Mechanics. Received January 26, 2019;
Accepted manuscript posted February 17, 2019. doi:10.1115/1.4042920

Harvesters Based on ZnO," Small, 9(20), pp. 3398-3404.

[18] Li, S., Liu, X., Li, R., and Su, Y., 2017, "Shear deformation dominates in the soft adhesive layers of the laminated structure of flexible electronics," International Journal of Solids and Structures, 110, pp. 305-314.

[19] Liu, H., Zhao, H., Li, S., Hu, J., Zheng, X., Li, R., Chen, Y., and Su, Y., 2018, "Adhesion - Free Thin - Film - Like Curvature Sensors Integrated on Flexible and Wearable Electronics for Monitoring Bending of Joints and Various Body Gestures," Advanced Materials Technologies, p. 1800327.

[20] Su, Y., Ping, X., Yu, K. J., Lee, J. W., Fan, J. A., Wang, B., Li, M., Li, R., Harburg, D. V., Huang, Y., Yu, C., Mao, S., Shim, J., Yang, Q., Lee, P. Y., Armonas, A., Choi, K. J., Yang, Y., Paik, U., Chang, T., Dawidczyk, T. J., Huang, Y., Wang, S., and Rogers, J. A., 2017, "In-Plane Deformation Mechanics for Highly Stretchable Electronics," Advanced materials, 29(8).

[21] Lee, Y. K., Jang, K.-I., Ma, Y., Koh, A., Chen, H., Jung, H. N., Kim, Y., Kwak, J. W., Wang, L., Xue, Y., Yang, Y., Tian, W., Jiang, Y., Zhang, Y., Feng, X., Huang, Y., and Rogers, J. A., 2017, "Chemical Sensing Systems that Utilize Soft Electronics on Thin Elastomeric Substrates with Open Cellular Designs," Advanced Functional Materials, 27(9), p. 1605476.

[22] Dae-Hyeong Kim, and Jong-Hyun Ahn, W. M. C., Hoon-Sik Kim, Tae-Ho Kim, Jizhou Song, Yonggang Y. Huang, Zhuangjian Liu, Chun Lu, John A. Rogers, 2008, "Stretchable and Foldable Silicon Integrated Circuits," Science, 320, pp. 507-511.

[23] Khang, D. Y., Jiang, H. Q., Huang, Y., and Rogers, J. A., 2006, "A stretchable form of single-crystal silicon for high-performance electronics on rubber substrates," Science, 311(5758), pp. 208-212.

[24] Su, Y., Li, R., Cheng, H., Ying, M., Bonifas, A. P., Hwang, K.-C., Rogers, J. A., and Huang, Y., 2013, "Mechanics of finger-tip electronics," Journal of Applied Physics, 114(16).

[25] Wang, S., Li, M., Wu, J., Kim, D.-H., Lu, N., Su, Y., Kang, Z., Huang, Y., and Rogers, J. A., 2012, "Mechanics of Epidermal Electronics," Journal of Applied Mechanics-Transactions of the Asme, 79(3).

[26] Su, Y., Wu, J., Fan, Z., Hwang, K.-C., Song, J., Huang, Y., and Rogers, J. A., 2012, "Postbuckling analysis and its application to stretchable electronics," Journal of the

Journal of Applied Mechanics. Received January 26, 2019;
Accepted manuscript posted February 17, 2019. doi:10.1115/1.4042920

Mechanics and Physics of Solids, 60(3), pp. 487-508.

[27] Hwang, S.-W., Tao, H., Kim, D.-H., Cheng, H., Song, J.-K., Rill, E., Brenckle, M. A., Panilaitis, B., Won, S. M., Kim, Y.-S., Song, Y. M., Yu, K. J., Ameen, A., Li, R., Su, Y., Yang, M., Kaplan, D. L., Zakin, M. R., Slepian, M. J., Huang, Y., Omenetto, F. G., and Rogers, J. A., 2012, "A Physically Transient Form of Silicon Electronics," Science, 337(6102), pp. 1640-1644.

[28] Song, J., 2015, "Mechanics of stretchable electronics," Current Opinion in Solid State & Materials Science, 19(3), pp. 160-170.

[29] Zhang, Y., Huang, Y., and Rogers, J. A., 2015, "Mechanics of stretchable batteries and supercapacitors," Current Opinion in Solid State & Materials Science, 19(3), pp. 190-199.

[30] Song, J., Feng, X., and Huang, Y., 2016, "Mechanics and thermal management of stretchable inorganic electronics," National Science Review, 3(1), p. 128.

[31] Jiang, H., Khang, D.-Y., Fei, H., Kim, H., Huang, Y., Xiao, J., and Rogers, J. A., 2008, "Finite width effect of thin-films buckling on compliant substrate: Experimental and theoretical studies," Journal of the Mechanics and Physics of Solids, 56(8), pp. 2585-2598.

[32] Song, J., Jiang, H., Liu, Z. J., Khang, D. Y., Huang, Y., Rogers, J. A., Lu, C., and Koh, C. G., 2008, "Buckling of a stiff thin film on a compliant substrate in large deformation," International Journal of Solids and Structures, 45(10), pp. 3107-3121.

[33] Kim, D. H., Liu, Z., Kim, Y. S., Wu, J., Song, J., Kim, H. S., Huang, Y., Hwang, K. C., Zhang, Y., and Rogers, J. A., 2009, "Optimized structural designs for stretchable silicon integrated circuits," Small, 5(24), pp. 2841-2847.

[34] Vanfleteren, J., Gonzalez, M., Bossuyt, F., Hsu, Y. Y., Vervust, T., De Wolf, I., and Jablonski, M., 2012, "Printed circuit board technology inspired stretchable circuits," MRS Bulletin, 37(03), pp. 254-260.

[35] Jahanshahi, A., Gonzalez, M., Brand, J. v. d., Bossuyt, F., Vervust, T., Verplancke, R., Vanfleteren, J., and Baets, J. D., 2013, "Stretchable Circuits with Horseshoe Shaped Conductors Embedded in Elastic Polymers," Japanese Journal of Applied Physics, 52(5S1), p. 05DA18.

[36] Lee, C. H., Jeong, J.-W., Liu, Y., Zhang, Y., Shi, Y., Kang, S.-K., Kim, J., Kim, J. S., Lee, N. Y., Kim, B. H., Jang, K.-I., Yin, L., Kim, M. K., Banks, A., Paik, U., Huang, Y., and Rogers, J.

Journal of Applied Mechanics. Received January 26, 2019;
Accepted manuscript posted February 17, 2019. doi:10.1115/1.4042920

A., 2015, "Materials and Wireless Microfluidic Systems for Electronics Capable of Chemical Dissolution on Demand," Advanced Functional Materials, 25(9), pp. 1338-1343.

[37] Su, Y., Wang, S., Huang, Y., Luan, H., Dong, W., Fan, J. A., Yang, Q., Rogers, J. A., and Huang, Y., 2015, "Elasticity of Fractal Inspired Interconnects," Small, 11(3), pp. 367-373.

[38] Xu, S., Yan, Z., Jang, K.-I., Huang, W., Fu, H., Kim, J., Wei, Z., Flavin, M., McCracken, J., Wang, R., Badea, A., Liu, Y., Xiao, D., Zhou, G., Lee, J., Chung, H. U., Cheng, H., Ren, W., Banks, A., Li, X., Paik, U., Nuzzo, R. G., Huang, Y., Zhang, Y., and Rogers, J. A., 2015, "Assembly of micro/nanomaterials into complex, three-dimensional architectures by compressive buckling," Science, 347(6218), pp. 154-159.

[39] Kim, D. H., Song, J., Choi, W. M., Kim, H. S., Kim, R. H., Liu, Z., Huang, Y. Y., Hwang, K. C., Zhang, Y. W., and Rogers, J. A., 2008, "Materials and noncoplanar mesh designs for integrated circuits with linear elastic responses to extreme mechanical deformations," Proc Natl Acad Sci U S A, 105(48), pp. 18675-18680.

[40] Lee, J., Wu, J., Shi, M., Yoon, J., Park, S. I., Li, M., Liu, Z., Huang, Y., and Rogers, J. A., 2011, "Stretchable GaAs photovoltaics with designs that enable high areal coverage," Advanced materials, 23(8), pp. 986-991.

[41] Dae-Hyeong, K., Jizhou, S., Won Mook, C., Hoon-Sik, K., Rak-Hwan, K., Zhuangjian, L., Huang, Y. Y., Keh-Chih, H., Yong-Wei, Z., and Rogers, J. A., 2008, "Materials and noncoplanar mesh designs for integrated circuits with linear elastic responses to extreme mechanical deformations," Proc Natl Acad Sci U S A, 105(48), pp. 18675-18680.

[42] Shin, G., Jung, I., Malyarchuk, V., Song, J., Wang, S., Ko, H. C., Huang, Y., Ha, J. S., and Rogers, J. A., 2010, "Micromechanics and advanced designs for curved photodetector arrays in hemispherical electronic-eye cameras," Small, 6(7), pp. 851-856.

[43] Wu, J., Liu, Z. J., Song, J., Huang, Y., Hwang, K. C., Zhang, Y. W., and Rogers, J. A., 2011, "Stretchability of encapsulated electronics," Applied Physics Letters, 99(6).

[44] Lan, L., Lin, H., Qiao, S., Yi, Z., Danto, S., Richardson, K., Musgraves, J. D., Lu, N., and Hu, J., 2014, "Integrated flexible chalcogenide glass photonic devices," Nature Photonics, 8(8), pp. 643-649.

[45] MingLi, JianhangXiao, JianWu, Rak-HwanKim, ZhanKang, YonggangHuang, and Rogers, J., 2010, "MECHANICS ANALYSIS OF TWO-DIMENSIONALLY PRESTRAINED

Journal of Applied Mechanics. Received January 26, 2019;
Accepted manuscript posted February 17, 2019. doi:10.1115/1.4042920

ELASTOMERIC THIN FILM FOR STRETCHABLE ELECTRONICS," Acta Mechanica Solida Sinica, 23(6), pp. 592-599.

[46] Dassault-Systèmes, 2010, "Abaqus analysis user's manual v.6.10. (Dassault Systèmes Simulia Corp., Rhode Island).".

Journal of Applied Mechanics. Received January 26, 2019;
Accepted manuscript posted February 17, 2019. doi:10.1115/1.4042920

Figure captions

Figure 1 Schematics of the island-bridge mesh structure of flexible electronics with laminated ribbons for interconnects (with permissions): a) a four-layer ribbon consisting of PI/Cr/Au/PI; b) a three-layer ribbon consisting of SU8/Au/SU8; c) a four-layer ribbon consisting of PI/metal/SiO_2/PI.

Figure 2 a) Schematic illustration of a laminated ribbon subjected to the distributed axial forces and bending moments. b) The cross section of the laminated ribbon.

Figure 3 a) Schematic illustration of the cross section of the double-layer ribbon. Comparison of the tensile/bending stiffness of the three models and 3D FEA, and the effects of the width: b1) $\nu_1=0, \nu_2=0.49$ for tensile stiffness; b2) $\nu_1=0, \nu_2=0.49$ for bending stiffness; c1) $\nu_1=-0.9, \nu_2=0.49$ for tensile stiffness; c2) $\nu_1=-0.9, \nu_2=0.49$ for bending stiffness.

Figure 4 The distribution of the normalized shear stress at the interface between the two layers along *x* axis: a) & b) $\nu_1=0$; c) $\nu_1=-0.9$.

Figure 5 The effects of Poisson's ratio ν_2 on the tensile/bending stiffness of the double-layer ribbon: a1) $\nu_1=-0.9$ for tensile stiffness; a2) $\nu_1=-0.9$ for bending stiffness; b1) $\nu_1=0$ for tensile stiffness; b2) $\nu_1=0$ for bending stiffness; c1) $\nu_1=0.5$ for tensile stiffness; c2) $\nu_1=0.5$ for bending stiffness.

Figure 6 The effects of Young's modulus E_2 and thickness t_2 on the tensile/bending stiffness of the double-layer ribbon. a1) E_2 on tensile stiffness; a2) E_2 on bending stiffness; b1) t_2 on tensile stiffness; b2) t_2 on bending stiffness.

Journal of Applied Mechanics. Received January 26, 2019;
Accepted manuscript posted February 17, 2019. doi:10.1115/1.4042920

Figure 1

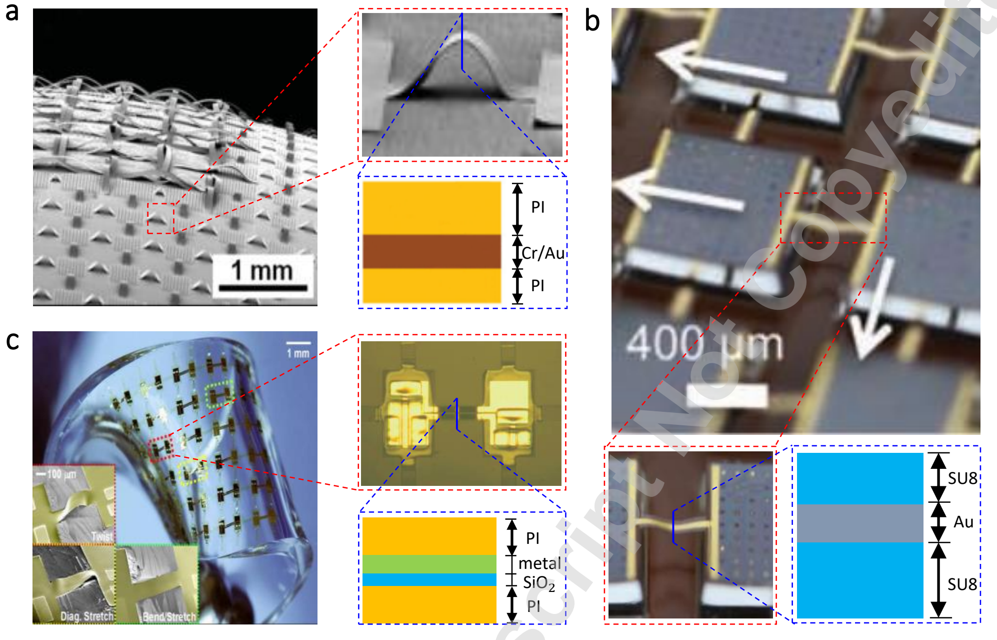

Journal of Applied Mechanics. Received January 26, 2019;
Accepted manuscript posted February 17, 2019. doi:10.1115/1.4042920

Figure 2

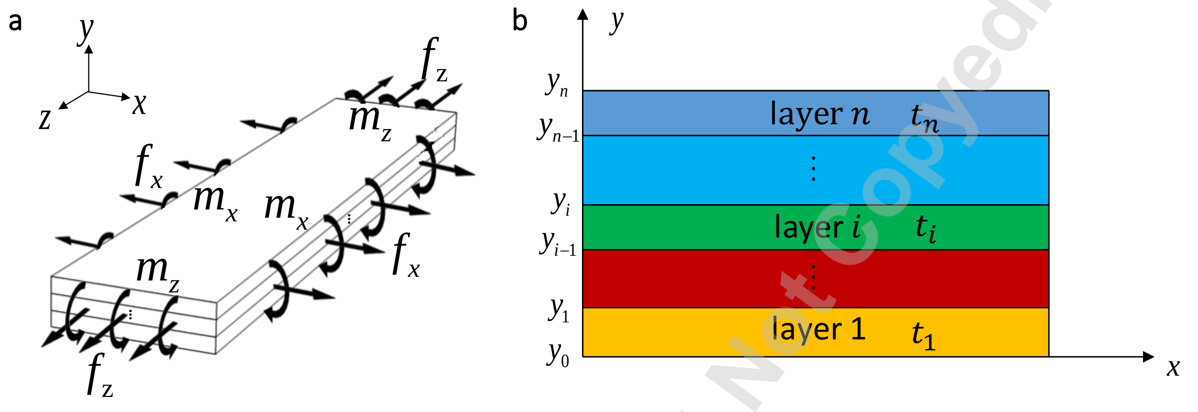

Journal of Applied Mechanics. Received January 26, 2019;
Accepted manuscript posted February 17, 2019. doi:10.1115/1.4042920

Figure 3

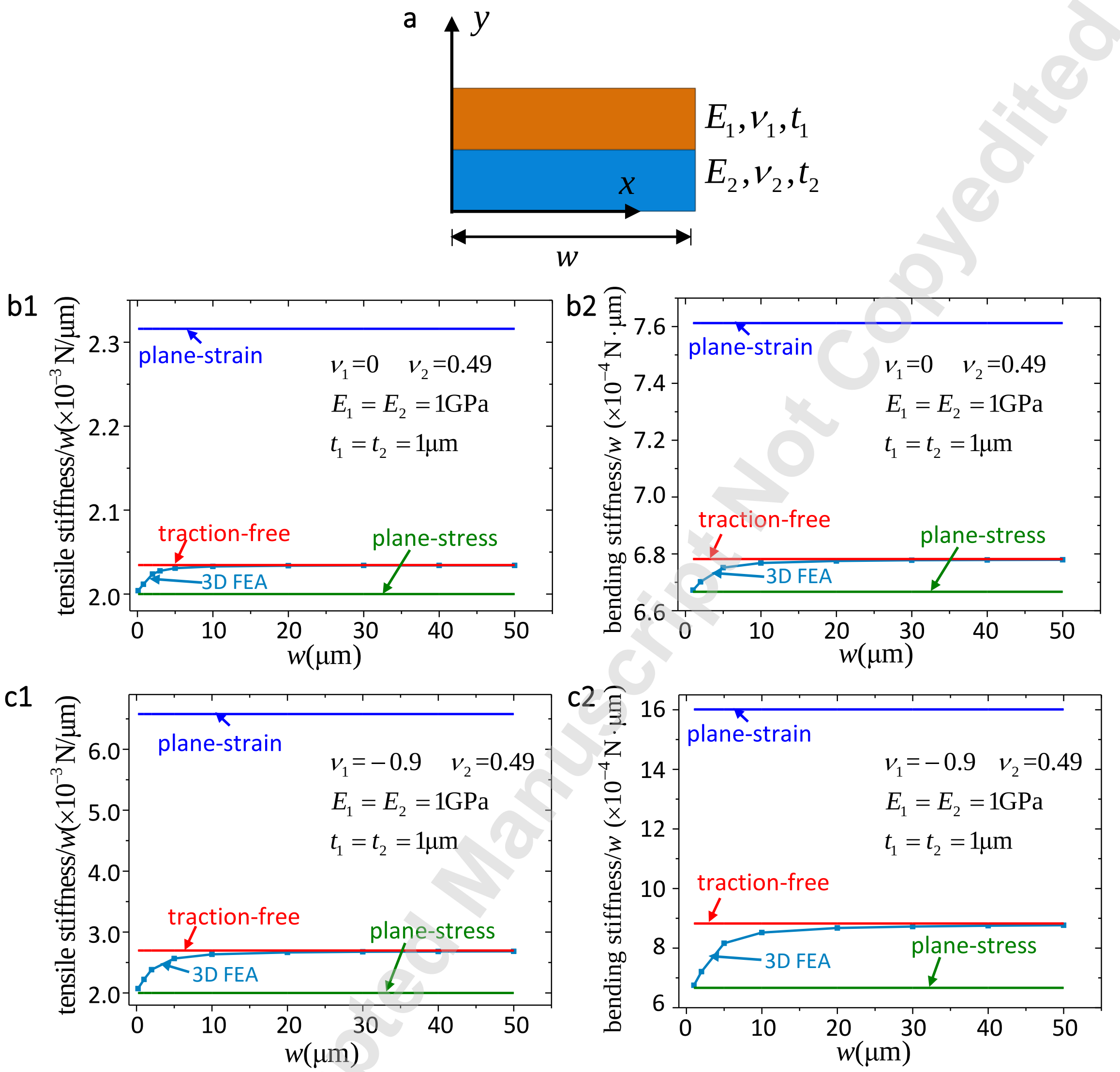

Journal of Applied Mechanics. Received January 26, 2019;
Accepted manuscript posted February 17, 2019. doi:10.1115/1.4042920

Figure 4

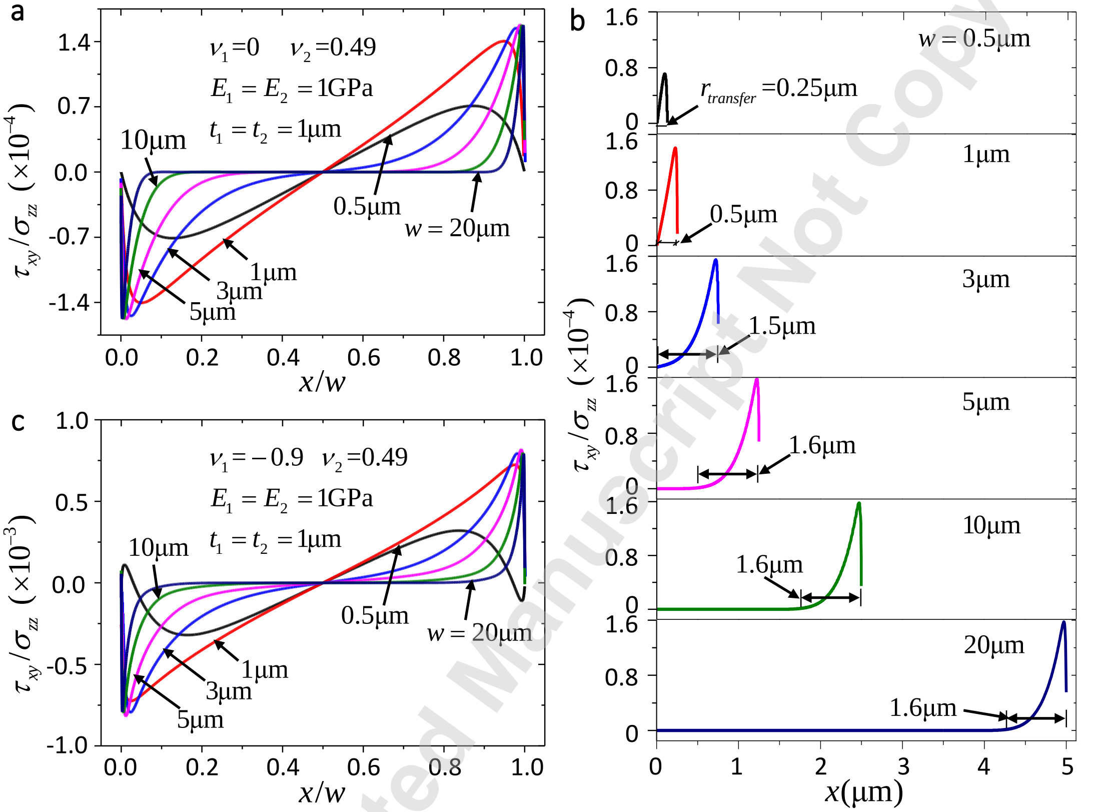

Journal of Applied Mechanics. Received January 26, 2019;
Accepted manuscript posted February 17, 2019. doi:10.1115/1.4042920

Figure 5

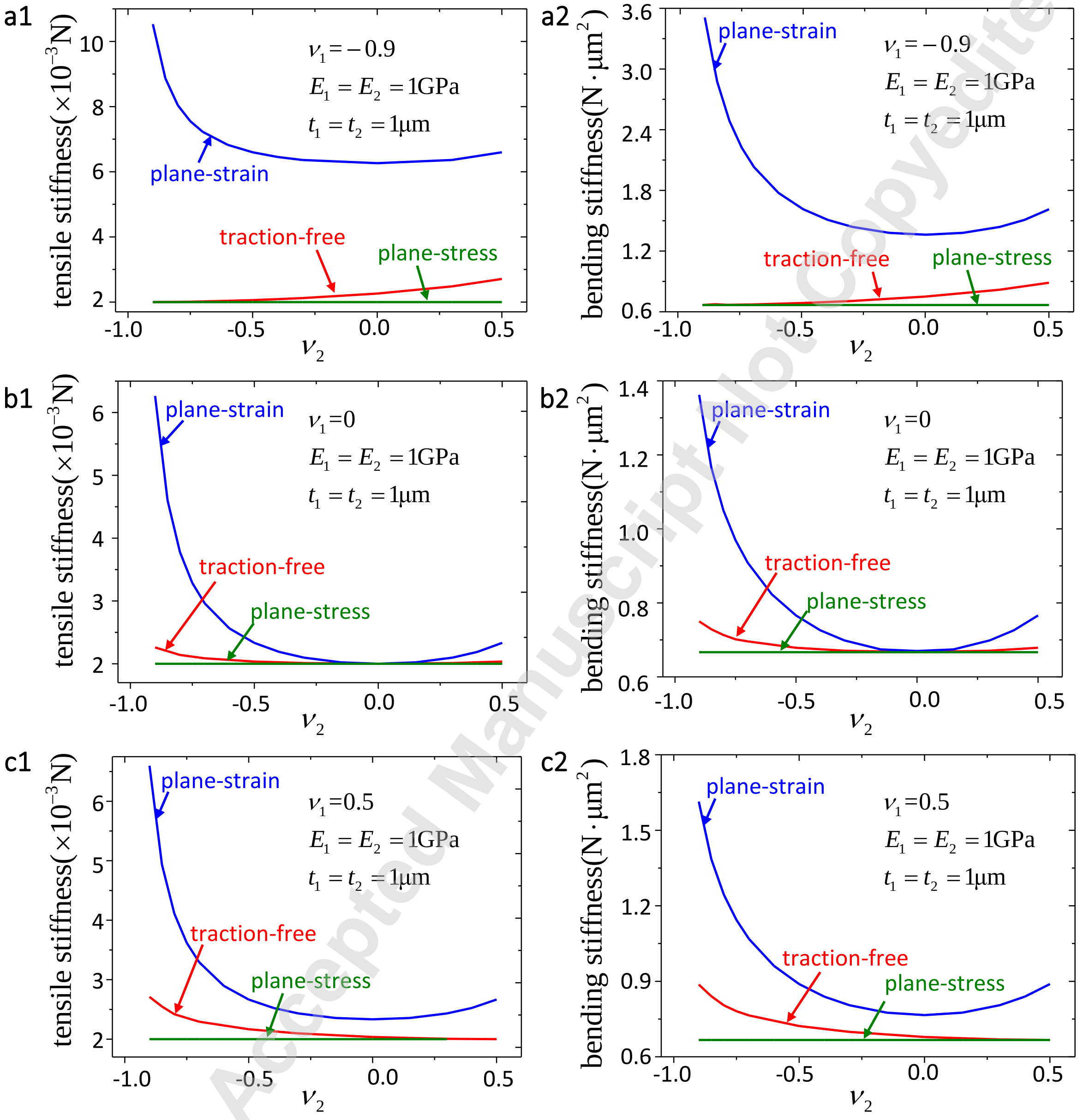

Journal of Applied Mechanics. Received January 26, 2019;
Accepted manuscript posted February 17, 2019. doi:10.1115/1.4042920

Figure 6